A Performance Comparison of WSS Switch Engine Technologies

Summary

This paper provides an overview of the currently prominent switch engine technologies used in wavelength selectable switches (WSS's) and illustrates how the majority of the critical characteristics of the WSS, the physical component size and port count, port isolation and cascaded channel passband width, are related to a pair of fundamental properties of the switch engine technology itself, namely the minimum spot size and the amount of scattering within the switch engine.

1 Introduction

Wavelength Selective Switches (WSS's) have become the established heart of the modern DWDM reconfigurable agile optical network. It serves as the optical component which is responsible for dynamically routing, blocking and attenuating all DWDM wavelengths within a network node. Therefore, the performance of this device is generally the one of the dominant attributes which define the performance of the overall network system. Thus, selecting a WSS with the sufficient performance is critical.

The high level functionality of the WSS is illustrated in Figure 1-1. It consists of a single common optical port and *N* opposing multi-wavelength ports where each DWDM wavelength injected into the common port can be routed to any one of the *N* multiwavelength ports, independent of how all other wavelength channels are routed. This wavelength provisioning is dynamic and is controlled through a digital communication interface on the WSS. The functionality of the WSS is optically bi-directional in that if multiple signals at the same DWDM wavelength, each injected into an independent port of the *N* ports, only one of these signals from one of the ports can be selected to be passed to the common port. In this case, all other channels at that same wavelength are blocked from reaching the common port. Additionally, each routed wavelength can be independently attenuated to allow for channel power control and equalization.

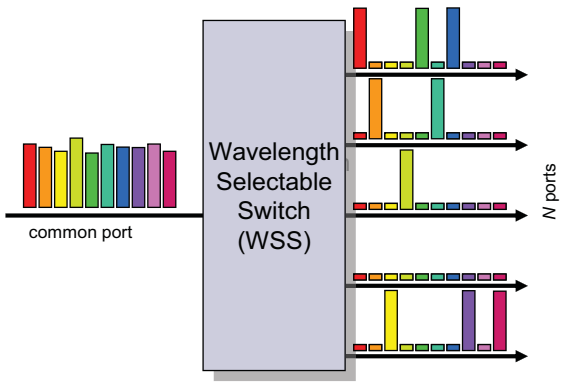

Figure 1-1: A functional diagram of a WSS. Wavelength channels launched into the common port are independently routed to any of the *N* output powers. Also, each channel can be independently attenuated for channel power equalization.

Figure 1-2 shows a typical node architecture of an agile optical network node incorporating a WSS. For each transmission fiber entering the node, an optical copy of all DWDM channels on that fiber is directed to one of the multiwavelength input ports of each WSS. The common ports of each WSS are directed to respective output transmission fibers leaving the node. Therefore, every DWDM channel present within the node is injected into every WSS. For each wavelength channel, selecting which signal is routed to the common port determines which particular signals will be routed along each particular transmission fibers out of the node.

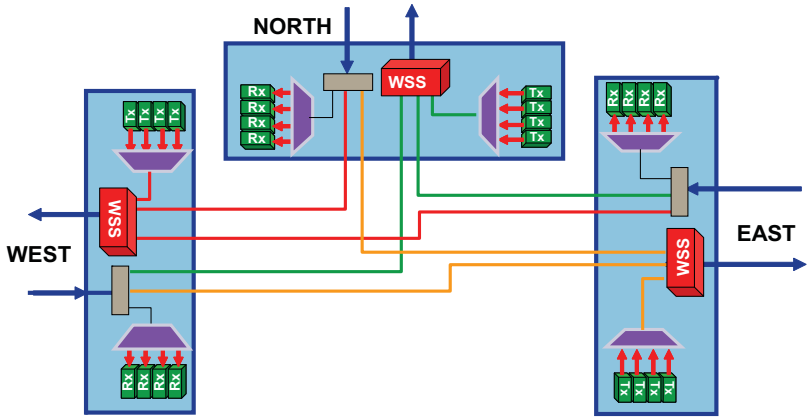

Figure 1-2: Typical node architecture of a 3 degree WSS enabled node

In performing these duties, there are several characteristics of the WSS's that directly affect the potential performance of the overall network. As the WSS is responsible for blocking all wavelengths not provisioned to continue on its respective fiber, the thoroughness of that blocking, or port isolation, is a critical performance parameter. Insufficient blocking will result in a degradation of the same-wavelength signal truly provisioned onto that fiber.

The WSS is also required to independently route closely spaced adjacent wavelength channels to different ports. To allow for the most signal bandwidth to be transmitted by each wavelength channel, the frequency width about each channel in which the optical signal is completely routed must be maximized and the amount of frequency space between the channels which is not fully routed must be minimized. Referred to as the channel bandwidth of the WSS, this parameter is critical as each signal is expected to pass through a significant number of WSS's such that the amount of bandwidth available for the signal to pass declines as a function of the number of WSS's passed. Therefore, to achieve superior system performance in a given network, it is necessary that both the port isolation and the channel bandwidth be as large as possible.

Currently, WSS components are supplied by several vendors and using several different arrayed switch engine technologies in conjunction with a diffraction grating based free-space-optics platform. In general and for each technology, the switching engine spatially directs the light of each wavelength channel between the common port and one of the *N* ports by changing the angle or position of the given wavelength channel's optical beam. The technologies that are currently being utilized to achieve this functionality are micro-electromechanical system (MEMS) mirror arrays, in single and two dimensional arrays [1-2], liquid crystal on silicon (LCoS) phased array beam steering [3], and liquid crystal (LC) based polarization beam deflection [4].

This paper will provide an overview of the different WSS switch engine technologies and describe how the fundamental properties of each technology influences the critical channel bandwidth and port isolation performance characteristics of the WSS constructed using that technology as well as

what levels of WSS isolation and bandwidths are necessary for a given system architecture and performance. Also, this paper will describe how the potential physical size of the WSS component and the number of ports depends upon the fundamental characteristics of the switch engine technology.

2 General WSS Design Considerations

A WSS is essentially an optical spectrometer with a switching engine element at the back end. Many of the classical spectrometer optical design limitations affect the design of a WSS; however, for devices to be used in telecommunication networks there are additional performance constraints such as wide passbands, physical device size and cost. Increasingly, the physical size of the component has become particularly important in the drive to increase equipment density and allow greater integration of additional functionality on a single linecard. The properties of the switching engine are integral to the overall optical design and therefore critically affect many of the performance and characteristics of the overall WSS.

Figure 2-1 shows a generic functional block diagram for a typical WSS device design. With the exception of the dispersion system, the optical components needed are highly dependent on the choice of switching engine.

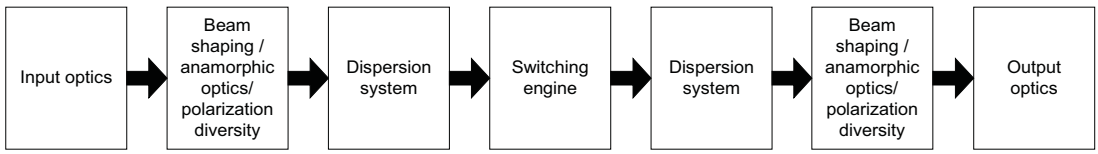

Figure 2-1: A functional block representing the typical sequence of optical elements of a WSS implementation. The beam shaping and polarization diversity functions can occur in a different order than shown.

2.1 Wavelength Channel Switching

In most current WSS designs, the ports are arranged as a one-dimensional array of fibers at the input/output, and this linear spatial separation of input/output fibers is mapped to an angular deflection at the switching engine. For each wavelength, beams from all ports converge to overlap at a single spot at the switching engine. To route a wavelength channel from the input port to an output port, the switching element (or elements) for that channel deflects the input beam so that it strikes the desired output fiber port. The direction of the port spreading may be either parallel or perpendicular to the direction of wavelength spreading produced by the grating. If it is parallel, then adding more ports increases the required dimension of the optics in the axis of the wavelength dispersion. If it is perpendicular (more common in current WSS designs), then adding more ports increases the dimension of the optics perpendicular to the axis of the dispersion.

2.2 WSS Component Size and Spot Size

The spectral shape of a channel (both passband and stopband widths) of a WSS is largely determined by the spectral resolution of the optical system. This can be expressed as a ratio of the distance between the centers of adjacent the channel switching elements (d) to the spot radius measured at the switching engine in the direction of the dispersion axis (ω). For the most part, the required d/ω ratio is independent of the type of switching engine chosen, and is typically >5. The channel spacing is related to d and the optical system parameters as follows:

channel spacing in GHz = angular dispersion of grating * f / d

where f is the focal length of the optical system. For a suitable d/ω ratio and a given channel spacing (which is fixed by requirement), the focal length scales linearly with spot radius (in the dispersion direction) as shown in Figure 2-2, and inversely with the angular dispersion of the grating. As the overall size of the optical system scales roughly with the focal length and the optical system size largely determines the physical size of the WSS component, for a minimum device size, the spot radius should be as minimum as possible. Furthermore, to achieve the widest channel bandwidth (i.e. the highest d/ω ratio). a minimum spot radius is equally desirable.

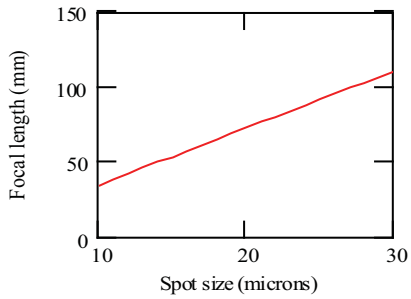

Figure 2-2: Relationship between spot size at the switching engine and spectrometer focal length for a particular choice of 1100 lines/mm diffraction grating and d/ω=6.

2.3 Channel Bandwidth and Spot Size

As shown in Figure 2-3, the WSS channel bandwidth performance needed dictates the spectral resolution (d/ω) required. For greater channel bandwidth, a higher d/ω ratio is needed. From here, it also follows that for a selected resolution and dispersive element, the focal length, and thus the overall optical system and component footprint, is proportional to beam size in the dispersion direction at the switching engine (Figure 2-2).

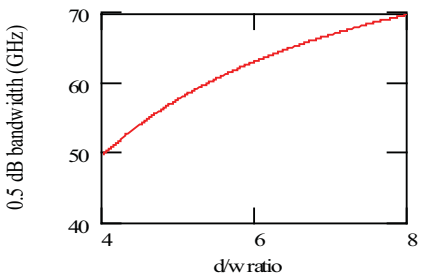

Figure 2-3: Relationship between 0.5 dB channel bandwidth and d/ω ratio, assuming 90% fill factor and a 100 GHz channel spacing.

2.4 Switch Engine Technologies and Minimum Achievable Spot Sizes

Some switching engine technologies require a minimum beam size to function properly, and thus place a limit on the minimum optical system length for a given channel passband width, channel spacing, and dispersive element [5]. The advantages of a small optical system size include a smaller overall module footprint, greater functional density, lower packaging cost (especially if the optical system requires hermetically sealing), and greater tolerance to mechanical shock and environmental conditions.

A binary LC switching engine is comprised of a stack of consecutive pairs of LC cells and polarization splitting elements. Each pair of LC cell and polarization splitting element provides a 1x2 switching functionality so that a cascade of R pairs results in a $1\times2R$ switch as shown in Figure 2-4. Within the stack, the beam must maintain a focus and therefore possess a depth of focus at least as long as the total optical thickness of the stack (RT/n where T is the physical thickness of one pair and n_i is the refractive index). Thus, this forces a minimum achievable beam radius of $\omega_{\min} = \sqrt{2\lambda/RT/\pi n_i}$. For typical 8-port WSS designs, the minimum beam radius needs be around 50 µm.

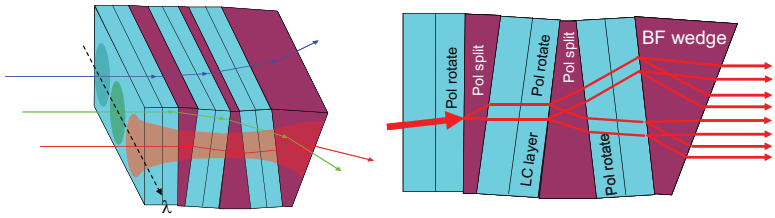

Figure 2-4: Illustration of a typical binary LC switching engine

A LCoS-based switch engine built uses an array of phase controlled pixels to implement beam steering by creating a linear optical phase retardation in the direction of the intended deflection (see Figure 2-5). This type of engine and other pixelated array switching engines require a beam radius in the direction of the dispersion that encompasses ≥2 pixels to average out the impact of the gaps between pixel elements which typically results in insertion loss ripple versus wavelength. For typical WSS designs, this leads to a minimum beam radius of around 15 µm.

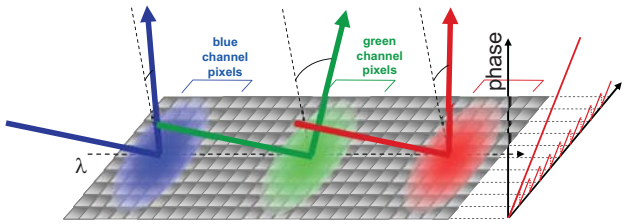

Figure 2-5: Illustration of a typical LCoS pixelated phase steering array

Another switch engine technology utilizes a similarly pixelated two-dimensional array of micro-MEMS reflective mirrors to perform the beam necessary beam steering (a derivative of the Texas Instruments DLP product line). In this case, the angle of the MEMS mirrors is changed to steer the beam; however, the current implementations only allow the mirrors to have two possible states. Therefore, there are only two potential angles in which to deflect the beam (see Figure 2-6). Similar to the LCoS switch engine and in order to avoid insertion loss ripple, the beam radius at the switch engine must be >2 pixels thereby limiting the minimum spot radius to a similar 15 µm.

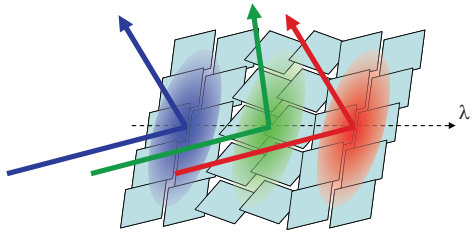

Figure 2-6: Illustration of a typical two dimension MEMS mirror array (DLP)

The final switch engine considered is one that utilizes a single array of MEMS reflective planar mirrors elements, each capable of continuous angular tilting in both axes, which is custom designed for WSS applications. One mirror element is dedicated to each wavelength channel resulting in continuous reflectivity across the channel with the only gaps occurring between channels (see Figure 2-7). Therefore, the minimum beam size in the dispersion direction at the surface of the mirror is not fundamentally limited by the switching engine itself. Instead, the obtainable minimum beam size is determined by the complexity tolerance of the optical design given the need for diffraction-limited optical performance and potentially the surface quality of the reflective mirrors. Therefore, a minimum beam radius of <10 μm can be readily achieved.

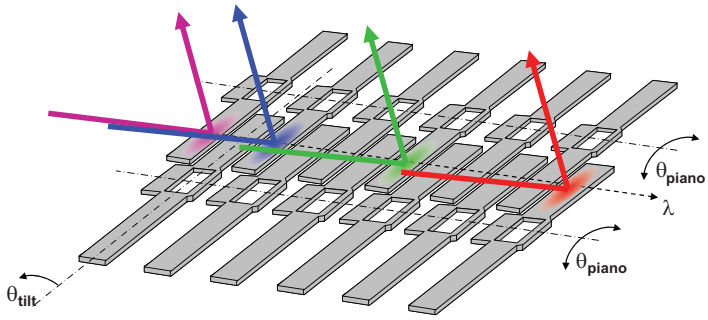

Figure 2-7: Illustration of a typical single dimension MEMS mirror array

In summary, three of the four prominent switch engine technologies have limitations on the minimum spot size at the switch engine which translate into limitations in the component dimensions or the channel bandwidth or places pressure on increasing the dispersion strength of the diffractive grating. However, the single dimension array of MEMS mirrors, being comprised of simple reflective mirrors, have no such fundamental spot size limitations, thus allowing the freedom to directly reduce the component size, improve the channel bandwidth and without requiring challenging stronger dispersive grating technology.

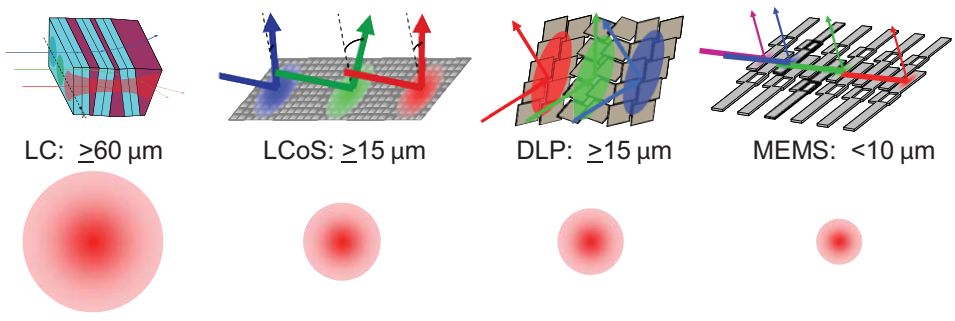

Figure 2-8: Comparison of typical minimum spot radii for various switch engine technologies

3 WSS Port Isolation and Switch Engine

3.1 Definition and General Causes

The port isolation of a WSS, for a given wavelength channel and port, is typically defined as the ratio of the insertion loss between the common port and the port in which the respective wavelength channel is routed to the insertion loss between the common port and the port in which that same wavelength is blocked (see Figure 3-1). Incomplete port isolation stems from two general causes.

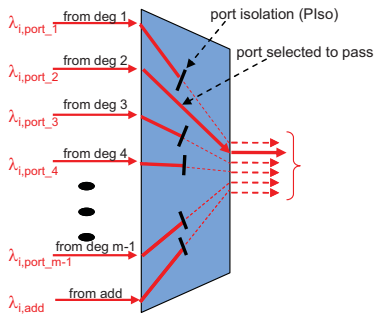

Figure 3-1: Port isolation in the WSS

The first cause is the imperfect deflection, or scattering, of light that is not intended to be coupled to the common port. That light, which is scattered in such a direction so as to strike the common fiber, will be coupled into that fiber resulting in the incomplete blocking of that signal (see Figure 3-2). Therefore, switch engines with the lesser amount of scattering will have the higher levels of port isolation. If the amount of scattering is generally constant across the channel actuator section, the minimum level of port isolation will nominally be equivalently constant versus wavelength across the channel band and typically be the same for each channel. Therefore, the characteristic level of scatter of the switch engine generally determines the maximum isolation the WSS can achieve.

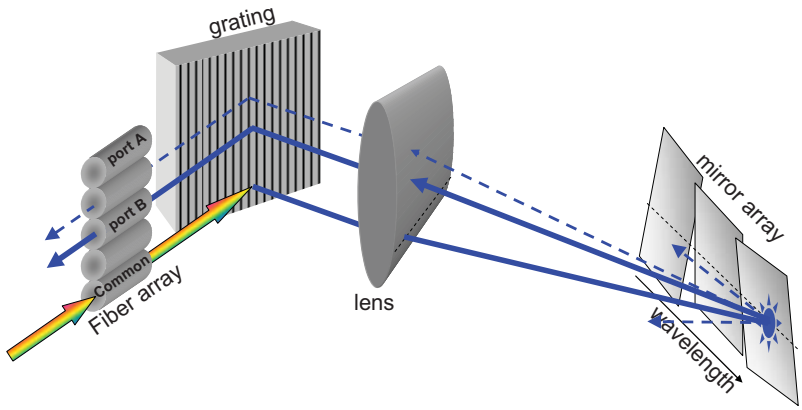

Figure 3-2: Illustration of how scattering from the switch engine (shown here as mirrors for simplicity) leads to reduced port isolation. Light scattered in the direction of an unintended port (dashed line) degrades port isolation.

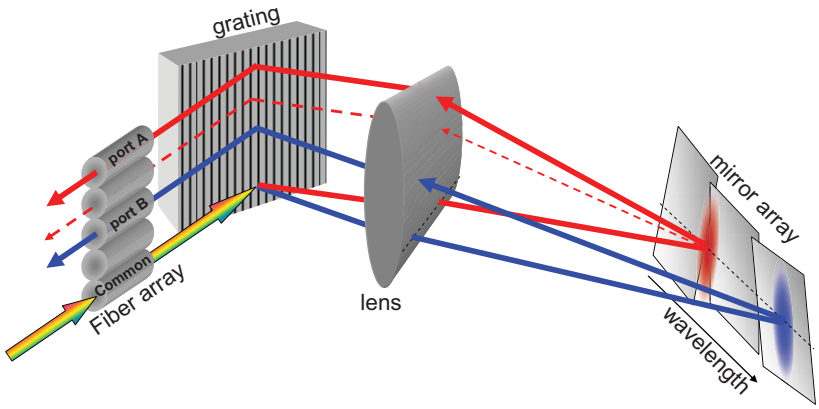

Figure 3-3: Illustration of how decreased port isolation towards the edges of the channel band is caused by the beam overlapping adjacent actuator regions (shown here as mirrors for simplicity). For those wavelengths where the beam overlaps two actuator regions (red beam), the beam is split and light is directed towards two output ports, one being the intended port (solid red line) and the other being an unintended port (dashed red line).

The second cause arises towards the edges of the channel passbands as the finite sized beam begins to overlap the adjacent actuator section of the switch engine and a portion of that beam is deflected directly to the unintended output fiber in which that adjacent actuator is positioned. This is illustrated in Figure 3-3. Therefore, to minimize the extent to which the decreased isolation extends into the channel passband, the ratio of the spot size to the width of the channel actuator (d/ω) needs to be as minimal as possible. When this ratio is smaller, for wavelengths towards the edges of the channel band, a greater portion of the beam remains within the actuator section and is therefore more fully deflected towards the proper port resulting in increased isolation. Therefore, with a lower ratio, the width of the area of maximum isolation within the channel band is wider. This is shown in Figure 3-4.

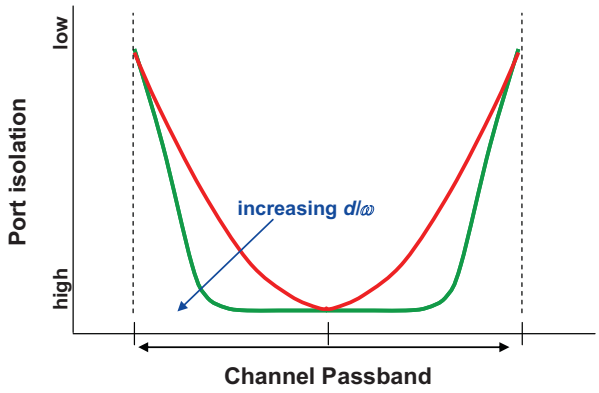

Figure 3-4: Illustration of how the port isolation decreases towards the edges of the channel passband and how that decrease is dependent upon the ratio of d/ω

3.2 Port Isolation in a Network System

Typically, in the architecture of a multi-degree reconfigurable optical add-drop multiplexer (ROADM) node, the DWDM signals present within each degree are launched into one of the *N* ports of an *N*x1 WSS (see Figure 3-5). For each wavelength channel, the WSS is provisioned to route the signal from the single desired port to the common output port, while blocking all other signals of that same wavelength, in all other ports, from reaching the common port. Within the WSS of each node and for each routed wavelength, interfering power can originate from each of the other *N*-1 WSS ports which are both connected to an installed degree and have an active signal present at that wavelength (of randomly oriented optical phase and polarization state). This interference is within the channel passband and therefore will co-propagate with the primary signal and accumulate with each node passed. To allow for positive channel power level equalization, a nominal attenuation of 4 dB for all routed channels is assumed.

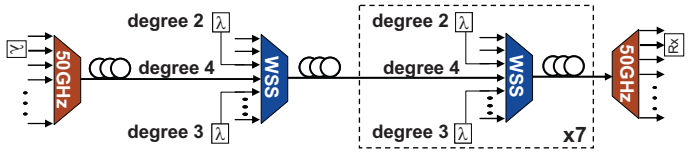

Figure 3-5: WSS-based multi-degree ROADM network

3.3 Port Isolation and 40 Gb/s Transmission

The demand for higher network capacity and greater spectral efficiency is driving the industry to transmit higher line rates (e.g. 43 Gb/s) over wavelength channels with a 50 GHz spacing. However, many 43 Gb/s modulation formats possess significant signal power across the entire 50 GHz channel passband. Therefore, the 50 GHz WSS components responsible for routing and blocking these wide 43 Gb/s signals must provide sufficient port isolation across the entire channel passband, unlike at lower line rates where the signals occupy only the central region of the passband [6]. Figure 3-6 shows a measured port isolation profile of a MEMS mirror based WSS for the case where adjacent DWDM wavelength channels are routed to dissimilar ports. While the isolation exceeds 50 dB at the center of the channel, it decreases towards the edges of the passband, thus allowing potentially damaging crosstalk interference to accumulate towards the edges of the channel. Separately, depending significantly upon the type of switch technology used within the WSS, a constant level of lesser isolation across the center of the channel can occur resulting in "flat-isolation" profiles. An example of such a profile is shown in the blue trace of Figure 3-6.

We have experimentally measured the system penalty arising from these two types of port isolation profiles (see Figure 3-6) in an eight node ROADM mesh network of 4-degree nodes carrying 43 Gb/s NRZ-ADPSK wavelengths [7,8].

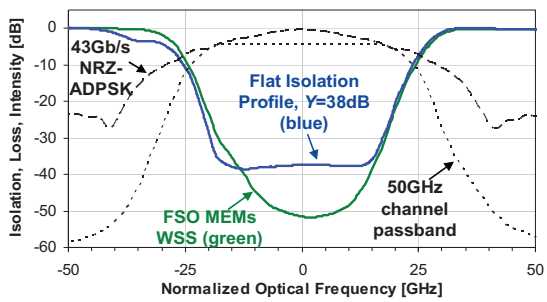

Figure 3-6: Measured port isolation profile of a single dimension MEMS mirror array based WSS (green trace) and of a WSS with a "flat-isolation" isolation profile with an isolation level of approximately *Y*=38 dB (blue trace). An unfiltered 43 Gb/s NRZ-ADPSK spectrum and a typical 50 GHz WSS channel passband are also shown.

We characterize the performance impairment and compare how the impairment depends upon the isolation levels at the channel center versus the edges of the passband [9].

3.4 Experimental Characterization of Port Isolation Requirements

3.4.1 Experimental Configuration

The experimental configuration used to emulate an 8 node system of 4 degree nodes is shown in Figure 3-7. The output of a 43 Gb/s NRZ-ADPSK transponder was passed through a 50 GHz multiplexing stage and then split into two copies. One was passed through an amplified cascade of four double-passed 50 GHz single dimension MEMS mirror array based WSS devices. The other copy was split into 16 mutually decorrelated signals and distributed to 8 fibers; each connected to one of two ports of each of the WSS's to represent the signals that must be blocked. Each fiber contained two decorrelated signal copies as each WSS was passed twice. Each WSS was provisioned to route adjacent wavelength channels to the common output port in order to produce the port isolation profiles all similar to the MEMS isolation profile of Figure 3-6 (green trace). The power levels of the interfering signal copies were equalized and their polarization states aligned to that of the primary signal. Optical noise was added to the signal before it was passed through a 50 GHz demultiplexing filter to the NRZ-ADPSK receiver for pre-FEC bit error rate measurement.

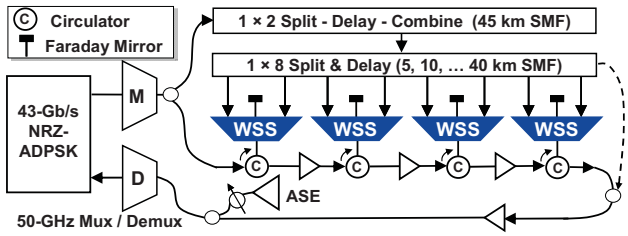

Figure 3-7: Schematic of the experimental configuration emulating an eight 4 degree node network

3.4.2 Results and System Level Analysis

Figure 3-8a displays the spectra of the total interfering crosstalk for the single dimension MEMS mirror array based WSS's (green trace) along with the primary signal, both measured at the Rx. Due to the high isolation at the channel center of the MEMS WSS's isolation profile, the crosstalk is greatest near the edges of the passband. The green trace (triangle markers) of Figure 3-9 plots the measured OSNR penalty (10^{-3} BER reference level) versus the total crosstalk power measured at the Rx, integrated over all frequencies and normalized by the total power of the primary signal. The total crosstalk power was modified (without change to its spectral structure) by uniformly adjusting the power levels of all interfering sources prior to their respective WSS. The transmission penalties caused by this crosstalk are relatively small. With a total relative crosstalk power of -12 dB, the OSNR penalty is less than 0.25 dB.

The WSS's and experimental configuration were then modified so that the WSS's port isolation profile possessed the "flat-isolation" profile as shown in the blue trace of Figure 3-6. The blue trace of Figure 3-8a shows the spectrum of the total interference power at the Rx with the amount of power near the center of the channel passband being considerably greater. The blue trace of Figure 3-8b (circle markers) shows the OSNR penalty versus the total relative interference power. From Figure 3-8b, it is clear that the impairment produced per unit of interference power is less when that power is concentrated towards the edges of the channel passband and the signal spectrum than when it resides about the center of the channel. For comparison, greater than 10 dB of additional interference power can be tolerated for the same penalty if that power is concentrated towards the edges of the channel

passband rather than if that power is located about the center. Conversely, for the same performance, greater than 10 dB less isolation can be tolerated towards the edges of the passband versus the center, especially as the power in the NRZ-ADPSK signal spectrum is naturally declining away from the channel center as well as filtered by downstream channel passbands.

To put these impairment characteristics into perspective, we measured the penalties resulting from unfiltered same-wavelength, in-band crosstalk interference generated by combining the 16 decorrelated interference signals directly with the primary signal after the WSS cascade using a passive optical coupler (dashed line in Figure 3-7).

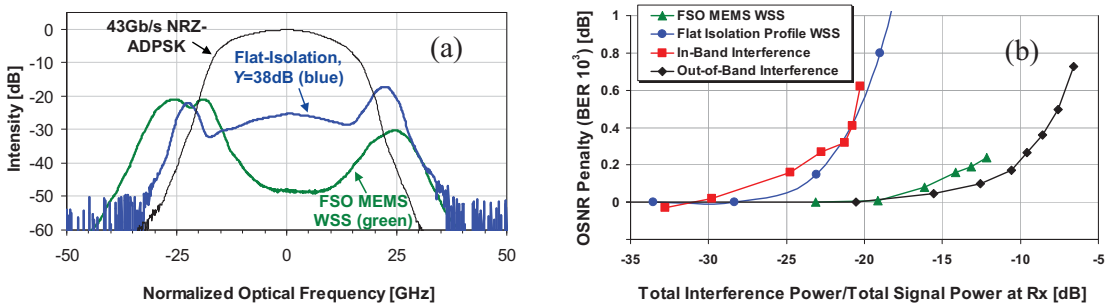

Figure 3-8: (a) Spectra of the resulting total interference crosstalk measured at the Rx for the single dimension MEMS mirror array based WSS (green) and the "flat-isolation" profile WSS (blue), and the NRZ-ADPSK signal. (b) OSNR penalty versus ratio of total average interference power for the single dimension MEMS mirror array based WSS (green triangles), the "flat-isolation" WSS profile (blue circles), in-band interference (red squares), and out-of-band interference (black diamonds)

Similarly, we created fully incoherent out-of-band crosstalk using 16 decorrelated interference signals generated from a second (50 GHz multiplexer filtered) NRZ-ADPSK transmitter tuned to an adjacent DWDM channel.

As can be seen in Figure 3-8b, the penalty from the same-wavelength, in-band interference closely follows the penalty from the "flat-isolation" profile WSS configuration suggesting that the "flat isolation" penalty is dominantly due to the centrally located interference power interacting coherently with the signal. However, the penalty due to interference from the fully out-of-band interference is rather similar to the penalty in the single dimension MEMS mirror array based WSS configuration supporting the conclusion that the interference power concentrated towards the edges of the channel passband results in a largely incoherent interaction with the signal.

The above results show that the critical portion of a WSS's port isolation profile is the isolation in the central region of the channel which is generally determined by the level of scattering characteristic of the switch engine technology. To extrapolate the system level penalty as a function of the WSS's isolation level and the number of nodes passed, one can assume the total in-band interference power (red trace with square markers of Figure 3-8b) to be composed of $2Z$ subcomponents of equal magnitudes. Each pair of subcomponents is assumed to be added in each of the Z WSS's passed, and each WSS has a center channel port isolation of Y dB. Thus, the total relative interference power (in decibel units) is equal to $-(Y-4)+10\log(2Z)$. Figure 3-9 plots the OSNR penalty versus Y for cascades of Z=8, 16 and 24 four degree nodes. As can be seen, an isolation of around 45 dB or better is needed to minimize the performance penalty. The penalties for the single dimension MEMS mirror array based WSS configuration (Y=52 dB) and the "flat-isolation" WSS configuration (Y=38 dB), are also plotted in Figure 3-9.

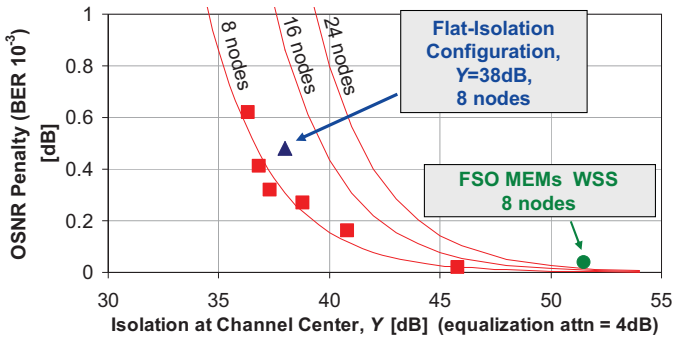

Figure 3-9: OSNR penalty versus channel center isolation level (*Y*) for networks with *Z*=8, 16 and 24 four-degree nodes

3.4.3 Port Isolation Dependence on Switch Engine Characteristics

Since the port isolation about the center of the channel band drives the level of system penalty, the sources of scattering and incomplete deflection of the various switch engine technologies are compared in Table 1. There are three general causes of scatter or imperfect deflection. The first cause is the number of optical surfaces encountered by the beam. As surfaces possess imperfections which scatter light, more surfaces encountered, will result in a larger the amount of cumulative scatter. All but the LC switch engine possess a very minor number of surfaces. However, the construction of the LC switch requires a number of surfaces with each switching stage and a number of stages are required to realize a higher port count device.

The second is the phase uniformity of the reflecting element within the beam. Lower uniformity results in greater scattering of the reflected the beam. The uniformities of the MEMS mirror surfaces and the LC cells are high and therefore the level of scattering is rather low. However, for pixelated switch engine technologies, the level of uniformity is less due to mirror pixel edges in the DLP and phase resets necessary in the LCoS phase profile.

The third limitation is the consequence of imperfect deflection and is applicable primarily to the LC switch engine. If the rotation and alignment of the polarization state at the output of the LC cell is not exact, the subsequent wedge will split that beam into two beams. However, by design, both of these beams are accurately aligned to the output fibers of the WSS. Therefore, if the rotation of the LC cell is incorrect, the port isolation will be compromised. For the other technologies, the accuracy of the steering of the beam does not impact the port isolation as the beam simply becomes less optimally coupled to the intended output fiber. However, that portion of the beam which misses the fiber does not couple into another output fiber as it is not physically near to any of the other output fibers.

Switch Engine Type / Cause of Scattering	MEMS	LC	LCoS	DLP
	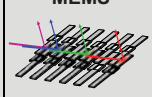	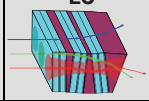	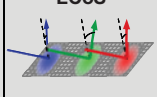	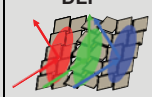
Consequence of Imperfect Steering Control	Light is thrown between ports (drift of angle)	Light is thrown directly into another port (incomplete polarization rotation)	Light is scattered to multiple ports (phase mask drift)	Not Applicable (hard MEMS stops)
Total Length of Edges per Channel	1 mm	2 mm (for 8 port device)	32 mm	16 mm (per pass)
Number of Surfaces	1 (MEMS mirror)	24 (for 8 port device)	3	3 (dual pass for attenuation)
Overall Port Isolation Performance	**Excellent ER** for all port counts	**Acceptable ER**, degrading with port count	**Poor ER**, degrading with port count	**Acceptable to Poor ER**

Table 1: Table providing to what extent scattering results for each of the switch engine types and a brief explanation of the aspect of the design is influencing the level of scattering.

3.5 Summary

Thus, for optimum port isolation performance, single dimension MEMS mirror arrays have the fundamental advantage as the level of scattering is very low given the surface quality of the mirror can be made sufficiently high, the mirror for each channel is not pixelated, and only a few surfaces are encountered by the beam.

4 Cascaded Channel Bandwidth

When a network employs more than one ROADM node, then some of the optical signals may pass through several WSS's before they reach their final destination. Hence, the question arises how many cascaded WSS's a signal can traverse before it becomes severely distorted by successive WSS optical filtering. This question becomes especially important for systems that transmit signals at data rates of 40 Gb/s or above through 50 GHz DWDM channels. As we shall show below, the bandwidth narrowing due to successive optical filtering not only depends on the spectral width of the WSS channel passband transfer function, but also on its shape. Also, a transfer function with a flat center section and steeply falling edges yields substantially wider cascaded bandwidth than a transfer function with gently falling edges. Hence, the shape of the transfer function also critically determines how many WSS's can be traversed by an optical signal. Finally, we will discuss how the passband shape depends on the switch engine technology used and the overall of the WSS.

4.1 Impact of Passband Shape

Signal distortions due to successive optical filtering usually occur when the cumulative bandwidth of the cascaded WSS's becomes equivalent or narrower than the spectrum of the transmitted optical signal. As a result, the tails of the signal spectrum are clipped and essential information may be lost in the process. The rate at which the cumulative bandwidth of the WSS cascade decreases with increasing number of WSS's depends solely on the shape of the transfer function of the individual WSS.

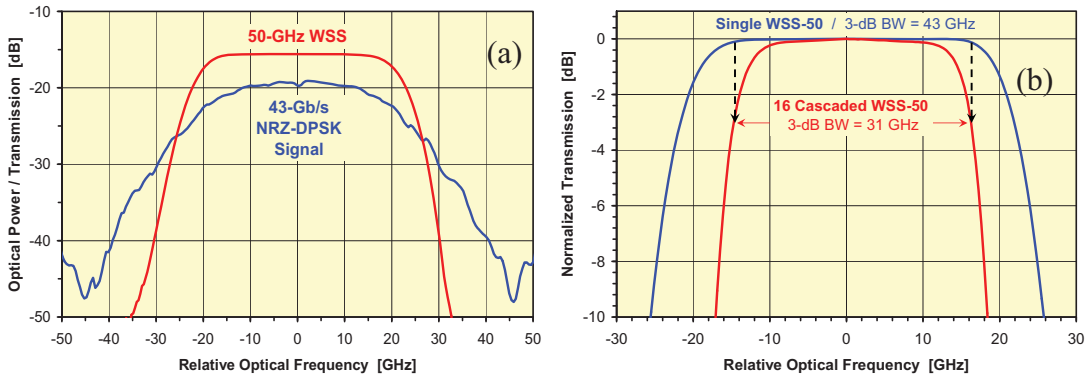

Figure 4-1: (a) Optical spectrum of an unfiltered 43 Gb/s NRZ-DPSK DWDM signal superimposed on the transfer function of a 50 GHz wavelength-selective switch (JDSU 5×1 MWS50). (b) Measured transfer function of a cascade of 16 nominally identical 50 GHz wavelength-selective switches (JDSU 5×1 MWS50). The 3 dB bandwidth of this cascade is determined by the 0.19 dB bandwidth of a single 50 GHz WSS.

This can be understood by considering a simple cascade of *M* identical WSS's, each having the same transfer function. The 3 dB bandwidth of the resulting overall transfer function is then simply given by the 3/*N* dB bandwidth of each individual WSS. With *M*=3, for example, the overall 3 dB bandwidth is equal to the 1 dB bandwidth of the individual WSS, and with *M*=6 it is equal to the 0.5 dB bandwidth of each WSS. Figure 4-1b shows a measurement of the cumulative transfer function of a cascade of 16 nominally identical WSS's, each having a 3 dB bandwidth of about 43 GHz (see Figure 4-1b). The 3 dB bandwidth of the 16 cascaded WSS's is determined by the 0.19 dB bandwidth of a single WSS, which is about 31 GHz. Therefore, the spectral transfer function of each WSS should be as flat and as wide as possible to allow cascading of a large number of WSS's.

4.2 Systematic and Random Amplitude Ripples

Signal distortions due to spectral filtering may not only arise from bandwidth filtering at the edges of the WSS transfer function but also from systematic amplitude ripples within the central portion of the transfer function. For example, if an amplitude dip of only 0.1 dB (or 2.3%) occurred at the center frequency of each WSS, then optical signals at this frequency would be attenuated by an additional 1.6 dB relative to the other portions for the signal when transmitted through a cascade of 16 WSS's. Note that randomly located amplitude ripples within the transfer function do not generally accumulate as rapidly as systematic ripples as they are not expected to repeatedly occur at the same wavelength.

Extended ROADM networks thus require WSS's with the widest possible bandwidth and with a flat-top transfer function exhibiting extremely small systematic amplitude variations.

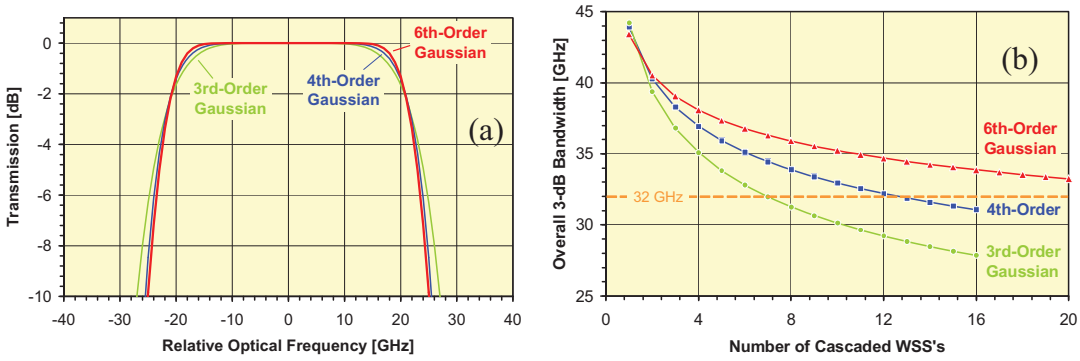

Figure 4-2: (a) Transfer functions of three 50GHz WSS's with different filter shapes, corresponding to super-Gaussian functions of order *n* = 3, 4 and 6. (b) Cumulative 3 dB bandwidth versus number of cascaded WSS's in a ROADM network for the three transfer functions shown in Figure 4-2a. WSS cascades with sixth order Gaussian transfer function clearly exhibit much less bandwidth narrowing than those with third order Gaussian transfer functions.

4.3 Gaussian Passbands of Different Shape

To demonstrate how important the flatness of the transfer function is, let us consider three WSS's with slightly different transfer functions (see Figure 4-2a). The three WSS's are assumed to exhibit the same 2 dB bandwidth but have different degrees of flatness across the central part of the transfer function. All three WSS's are assumed to have super-Gaussian transfer functions of the form $\exp - (f - f_0 / \Delta f)^{2n}$ but of different order n which determines the transfer function shape, wherein f is the optical frequency, f_o denotes the center frequency of the WDM channel, and Δf determines the bandwidth. The first transfer function has n=3, which is typical for planar waveguide based devices (and a 50 GHz channel spacing). The second transfer function with n=4 is slightly flatter and characteristic of earlier generation free-space single dimension MEMS mirror array based devices, whereas the third transfer function with n=6 represents state-of-the-art single dimension MEMS mirror array based WSS's and exhibits the steepest edges and the flattest central portion. At first glance, the differences between these three transfer functions appear relatively small. However, when several of these devices are cascaded as in a ROADM network, together they result in substantially different cumulative bandwidths, as can be clearly seen in Figure 4-2b.

When more than three WSS's are traversed, the sixth order Gaussian transfer function always yields the widest overall 3 dB bandwidth and, hence, allows the most devices to be concatenated. For example, if the optical signal requires a 3 dB bandwidth of at least 32 GHz, which is typical for 40 Gb/s NRZ-DPSK signals (see Figure 4-3, less bandwidth is typically needed for lower data rate signals), then it can traverse only up to seven third order Gaussian WSS's transfer function, but up to 12 WSS's with a fourth order transfer function and more than 20 WSS's with a sixth order transfer function. As it is expected that many of the current 10 Gb/s systems will eventually be upgraded to line rates of 40 Gb/s or even 100 Gb/s, it is extremely important to choose a WSS that exhibits the flattest and widest available transfer function.

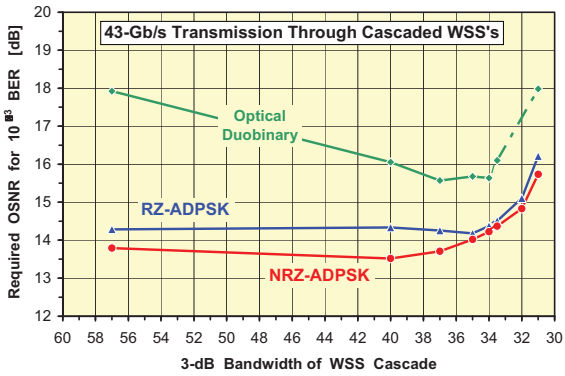

Figure 4-3: Optical signal to noise ratio (OSNR) penalties for three different 43 Gb/s signals passing through up to 16 cascaded 50 GHz WSS's. The three curves are plotted versus the cumulative 3 dB bandwidth of the WSS cascade and correspond to three different modulation formats: optical duobinary, RZ-ADPSK and NRZ-ADPSK.

4.4 Effect of Random Passband Center Frequency Shift

The above analysis assumes that all WSS passbands are identical and exhibited the same transfer function for all WSS input/output ports and DWDM channels. In practice, this is usually not the case. While shape and width of the transfer function typically vary only slightly from channel to channel and from device to device (and typically can be ignored), significant variations in the center frequency of each channel can occur. These variations arise from optical components imperfections, subtle misalignment of the optical system occurring during manufacturing, and from internal or environmental stress. In addition, one may expect certain systematic and random frequency shifts that change slowly with time and temperature.

We have performed an extensive analysis of a very large number of manufactured WSS devices and found that the worst-case frequency shift in any of the DWDM channels and ports of a single 50 GHz single dimension MEMS mirror array based WSS can be described by a systematic frequency shift of 1.1 GHz, and an additional randomly distributed shift with a Gaussian probability distribution and a standard deviation of 1.0 GHz. It should be noted that these numbers characterize the worst-case frequency shift in a single device and, therefore, are not representative of the typical frequency shifts in a WSS, which are substantially smaller.

If the frequency shifts were identical in all DWDM channels and devices, then the only effect in a WSS cascade would be a similar frequency shift in the overall transfer function of the concatenated WSS's. However, the frequency shifts in the worst-case wavelength channel have a random component in addition to the 1.1 GHz systematic shift. Therefore, the resulting frequency shift in the cumulative transfer function of a WSS cascade is randomly distributed and depends on the particular devices used in the cascade. Moreover, the fact that the transmission bands in the various devices are randomly shifted also gives rise to significant additional bandwidth narrowing in the overall transfer function of the cascade, as depicted schematically in Figure 4-4. Just like the overall frequency shift, the overall bandwidth narrowing depends on the particular devices employed in the cascade and, thus, varies randomly.

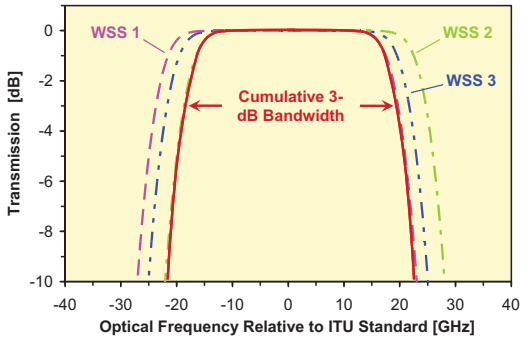

Figure 4-4: Random center frequency shifts in the elements of a WSS cascade cause additional bandwidth narrowing, as shown here schematically for 3 concatenated WSS's.

4.5 Statistical Modeling of Cascaded Bandwidths

For Gaussian transfer functions, it is possible to derive simple analytic expressions for the statistical distribution of the overall frequency shifts and bandwidths. The transfer function a single passband with random center frequency shift is then described by

$$\exp\left\{-\left[\frac{(f-\mu_i)^2}{2\sigma^2}\right]^n\right\},$$

wherein f denotes the relative optical frequency and $\mu_i = \mu_o + \Delta\mu_i$ the (undesired) systematic and random center frequency shifts due to optical misalignment, mechanical stress, aging, and temperature, with μ_o representing the systematic and $\Delta\mu_i$ the random shifts, respectively. Since the frequency shifts are small compared with the optical bandwidth of the transfer function, i.e. $\Delta\mu_i << \sigma$, we may approximate the exponent of the Gaussian transfer function as

$$\left[\frac{(f-\mu_i)^2}{2\sigma^2}\right]^n \approx \left[\frac{(f-\mu_0)^2}{2\sigma^2}\right]^n - 2n\Delta\mu_i\,\frac{(f-\mu_0)^{2n-1}}{\left(2\sigma^2\right)^n} + n(2n-1)\Delta\mu_i{}^2\,\frac{(f-\mu_0)^{2n-2}}{\left(2\sigma^2\right)^n} - \ldots\ .$$

For a cascade of M concatenated WSS's, this expression simply becomes

$$M\left[\frac{(f-\mu_0)^2}{2\sigma^2}\right]^n - 2n\sum_{i=1}^{M}\Delta\mu_i\,\frac{(f-\mu_0)^{2n-1}}{\left(2\sigma^2\right)^n} + n(2n-1)\sum_{i=1}^{M}\Delta\mu_i{}^2\,\frac{(f-\mu_0)^{2n-2}}{\left(2\sigma^2\right)^n} - \ldots\ ,$$

wherein the random variable $\sum_{i=1}^{M}\Delta\mu_i$ exhibits a Gaussian probability density function (PDF) with zero mean value and standard deviation $\sigma_\mu\sqrt{M}$, where σ_μ denotes the standard deviation of the random frequency shifts in the individual WSS's. To first order, therefore, the transfer function of M cascaded WSS's can be approximated by the expression

$$\exp\left\{-N\left[\left(f-\mu_0-\frac{1}{N}\sum_{i=1}^{N}\Delta\mu_i\right)^2\Big/2\sigma^2\right]^n\right\}\ ,$$

which describes the systematic and random frequency shifts in the overall transfer function (but not the corresponding bandwidth narrowing). Not surprisingly, the average frequency shift in the overall transfer function is identical to the systematic frequency shift in the individual WSS's (μ_o). However, the random frequency shifts in the overall transfer function, which are described by $\frac{1}{M}\sum_{i=1}^{M}\Delta\mu_i$, are generally smaller than those in the individual WSS's, because they tend to partially compensate each other. The standard deviation of the overall center frequency shifts is given by $\sigma_\mu/\sqrt{M}$ and, hence, decreases with the number of cascaded devices. Note that the overall frequency shift it is independent of *n*. Thus, it does not depend on the shape of the transfer function.

The first-order approximation of the overall transfer function does not include the additional bandwidth narrowing caused by the random center frequency shifts in the individual WSS's. For this we need a second-order approximation, which yields for the transfer function of *M* cascaded WSS's

$$\exp\left\{-M\left[\left(f-\mu_0-\frac{1}{M}\sum_{i=1}^{M}\Delta\mu_i\right)^2\Big/2\sigma^2+\frac{(2n-1)}{M}\sum_{i=1}^{M}\Delta\mu_i{}^2\Big/2\sigma^2\right]^n\right\},$$

wherein the random variable $\sum_{i=1}^{M}\Delta\mu_i^2$ has a non-vanishing mean of $\sigma_\mu{}^2 M$. Its PDF becomes approximately Gaussian for a large number of cascaded WSS's, i.e. for $N>>1$. Therefore, on average, the overall transfer function can be approximated as

$$\exp\left\{-M\left[\frac{(f-\mu_0)^2}{2\sigma^2}+\frac{(2n-1)\,\sigma_\mu{}^2}{2\sigma^2}\right]^n\right\},$$

wherein the second term indicates significant bandwidth narrowing, in particular for Gaussian transfer functions of high order, i.e. for $n>>1$.

4.6 Monte-Carlo Simulations of Cascaded Bandwidths with Random Frequency Shifts

The analytical results derived above have been confirmed by extensive Monte-Carlo simulations of the statistical distributions of the overall center frequency shifts and 3 dB bandwidths. In these calculations, 15,000 statistically independent WSS cascades were evaluated, wherein each cascade comprised up to 20 devices having systematic frequency shifts of μ_o=1.1 GHz and random frequency shifts $\Delta\mu$ with a standard deviation of σ_μ=1.0 GHz (see Figure 4-5).

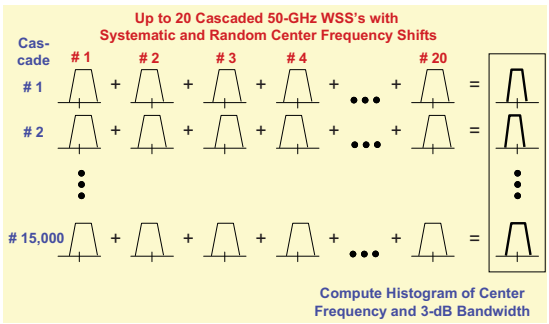

Figure 4-5: Numerical procedure for evaluating the statistical distributions of the overall center frequency shifts and 3 dB bandwidths of up to 20 cascaded WSS's, using a worst-case stochastic model for the random frequency shifts in the individual WSS's. Overall frequency shifts and bandwidths are calculated for 15,000 statistically independent WSS cascades.

These simulations also assume that one WSS in the cascade was operated at an elevated (but otherwise unspecified) temperature that causes the largest possible systematic frequency shift of μ_o=2.1 GHz. This additional frequency shift was included to assess the worst-case impact of a single defective environmental temperature controller in the network. However, our calculations show that the additional, temperature-induced frequency shift in a single WSS has only a small effect on the distributions of the overall frequency shift and 3 dB bandwidth. For longer WSS cascades it becomes negligible.

Figure 4-6a displays examples of the statistical distribution of the overall frequency shifts in a WSS cascade with sixth order Gaussian transfer function. As expected from the analytic model above, the overall frequency shift always exhibits a Gaussian PDF whose width decreases with increasing number *M* of concatenated WSS's. Also shown in Figure 4-6a is the average frequency shift as a function of cascaded devices as well as the 3σ value of the frequency variations (which includes 99.7% of all frequency shift occurrences). The average frequency shift is highest after the first WSS (because of the temperature-induced offset of 2.1 GHz) but quickly decreases with increasing *M* and is essentially equal to μ_o=1.1 GHz after about 10 concatenated WSS's. Likewise, the 3σ range of the frequency variations decreases rapidly from ±3 GHz after the first WSS to less than ±1 GHz after 10 WSS's.

Figure 4-7a then displays the corresponding statistical distributions of the cumulative 3 dB bandwidth of the WSS cascade. In general, the PDFs for the 3 dB bandwidth are asymmetric and non-Gaussian, although they approach a Gaussian function for very large *M*. Their width is largest after two concatenated devices (because of the large systematic frequency offset in the first WSS) and decreases only slowly with increasing *M*. On average, the 3 dB bandwidth is not much smaller than it would be without the random frequency shifts in the individual WSS's, as shown in Figure 4-2b, although the difference increases slowly with increasing number of concatenated WSS's (for *M*=20 it is still less than 0.5 GHz). However, the probability for much larger bandwidth reductions to occur is fairly high, because of the long tails in the asymmetric PDFs: at *M*=2, for example, there is a 0.15% chance that the random frequency shifts in the individual WSS's cause bandwidth narrowing in excess of 2.5 GHz. Although this range decreases slowly with increasing *M*, the impact of the additional bandwidth reduction on the transmission performance is higher at large *M*, where the shape-induced bandwidth reduction is already large.

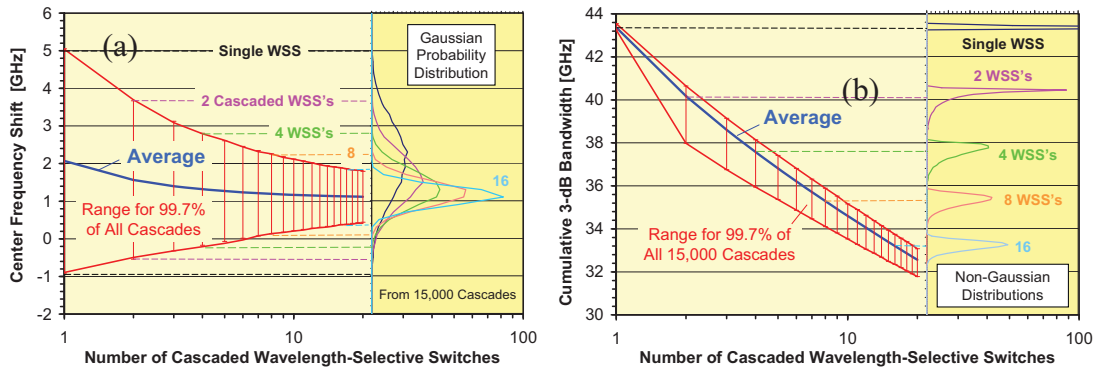

Figure 4-6: (a) Statistical distributions of the overall center frequency shifts in a cascade of up to 20 WSS's with sixth-order Gaussian transfer function. The standard deviation for the random frequency shifts in each WSS is 1.0 GHz, whereas the systematic frequency shift is 2.1 GHz in the first WSS and 1.1 GHz for all other devices. The left graph displays the average frequency shift in the 15,000 evaluated cascades (blue curve) and the 3σ values of the corresponding distributions (red curves) as a function of cascaded devices, while the inset shows examples of the Gaussian PDFs. (b) Statistical distributions of the overall 3 dB bandwidth of a cascade of up to 20 WSS's with sixth order Gaussian transfer function. The random and systematic frequency shifts in each WSS are the same as in Figure 4-6a. The left graph displays the average 3 dB bandwidth of the 15,000 evaluated cascades (blue curve) and the equivalent 3σ values of the corresponding statistical distributions (red curves) as a function of cascaded devices, while the inset shows examples of the PDFs for 1, 2, 4, 8, and 16 cascaded WSS's. Note that the PDFs become Gaussian for very long WSS cascades.

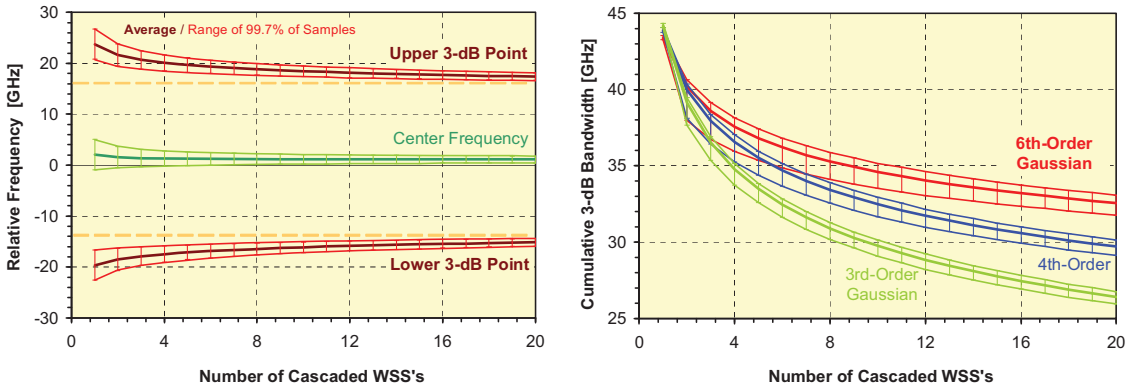

Figure 4-7: (a) Statistical distribution of the upper and lower 3 dB points of the overall transfer function versus number of cascaded WSS's having sixth order Gaussian transfer function. The bold curves display the average bandwidth and the thin curves the 99.7%-probability ranges. Also shown is the distribution of the center frequency shift. Even after 20 cascaded WSS's, a clear 3 dB bandwidth of 30 GHz is available with at least 99.7% probability (dashed lines). (b) Comparison of the 3 dB bandwidth evolution in WSS cascades with third, fourth, and sixth order Gaussian transfer function and similar random center frequency shifts. The bold curves display the average bandwidth and the thin curves the 99.7% probability ranges. For any given number of cascaded WSS's, the sixth order Gaussian transfer function, at least on average, always yields the widest bandwidth.

To estimate the spectral narrowing that may be experienced by an optical signal transmitted through such a WSS cascade, we have plotted in Figure 4-7b the 99.7% ranges for the upper and lower 3 dB points in the overall transfer function versus the number of cascaded WSS's. Because of the average center frequency shift, the average 3 dB points are offset by about 1 GHz from the center of the DWDM channel. Thus, an optical signal centered in the middle of the DWDM channel may experience asymmetric filtering, which becomes more severe as the number of WSS's increases. After 20 WSS's, the upper 3 dB point is likely to be offset by at least 16 GHz from the center of the channel and the lower 3 dB point is offset by at least 14 GHz in the opposite direction, yielding a total bandwidth of 30 GHz.

4.7 Impact of Passband Shape on Cascaded Bandwidth

One may argue that flat-top transfer functions with steeply declining edges, like the sixth order Gaussian considered above, are more sensitive to random center frequency shifts than more 'rounded' transfer functions, like the third order Gaussian shown in Figure 4-2. Also, one might think that this higher sensitivity may offset, at least partially, its substantially superior bandwidth narrowing behavior in cascaded ROADM networks. To address this question, we have repeated the statistical analysis described above for WSS's with the third and fourth order Gaussian transfer functions sown in Figure 4-2, using the same systematic and random frequency shifts for the individual WSS's. Figure 4-7b displays the 3dB bandwidth distributions for these transfer functions and compares them with those obtained for the sixth order Gaussian function. Clearly, for any given number of cascaded WSS's, the third order Gaussian transfer function exhibits the smallest range of bandwidth variations, but it also yields by far the smallest average bandwidth. This is especially the case at large M (i.e. $M \geq 4$), where the average 3 dB bandwidth is substantially lower than the 99.7% range of worst-case bandwidth calculated for the fourth or even sixth order Gaussian transfer functions. Therefore, Figure 4-7b clearly indicates that higher-order transfer functions always yield the widest cascaded bandwidth.

To show that this is not just the case for the particular magnitude of random center frequency shifts considered in Figure 4-6 through Figure 4-7 above, we have varied the standard deviation of these frequency shifts over a wide range and plotted the minimal 3 dB bandwidth obtained or exceeded in 99.85% of all 16 WSS cascades versus the magnitude of the standard deviation in Figure 4-8. The

results of these calculations clearly demonstrate that the sixth order Gaussian transfer function always yields the widest cascaded bandwidth, even if the magnitude of the random frequency shifts was increased by a factor of two or four. The curves also show that increasing the order of the Gaussian transfer function from 4 to 6, for example, is a much more effective method for achieving wider cascaded bandwidth than completely eliminating the random frequency shifts (the former gives rise to a 10% increase in bandwidth while the latter merely yields a 3% increase).

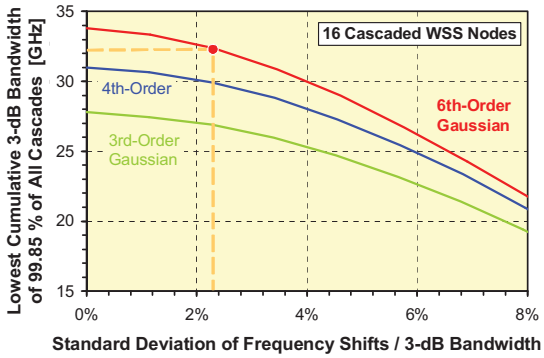

Figure 4-8: Dependence of the lower range of the overall 3 dB bandwidth variations with the magnitude of the standard deviation of the random center frequency shifts in the individual WSS's, calculated for a cascade with 16 devices having third, fourth, and sixth order Gaussian transfer functions. The red dot indicates the standard deviation considered in Figure 4-6 and Figure 4-7 above.

4.8 Choice of Switching Engine Technology

As we have seen above, the shape of the transfer function is a critical parameter for obtaining the widest possible cascaded bandwidth. The more rectangular the individual passbands are, the more WSS's may be employed in any given network. By and large, the passband shape of a WSS is determined by the optical technology used in its switching engine. For a given diffraction efficiency of the grating, the spacing of the mirrors determines the optical channel spacing, the width of the mirrors determines the bandwidth of the channels, and the spot size on the mirror determines the steepness of the passband edges. As shown schematically in Figure 4-9, for a given channel actuator dimension, a narrower spot size yields much steeper edges than a wider spot size. Similarly, the larger the ratio of the actuator to the spot radius (d/ω), the shape of the passband will be characterized by an increasing order Gaussian (n). Therefore, for best cascaded bandwidth (and smallest component dimensions), one desires the smallest potential spot size at the switch engine. See section 2.4 and Figure 2-8 for an overview of the minimum spot size tolerated by the various switch engine technologies.

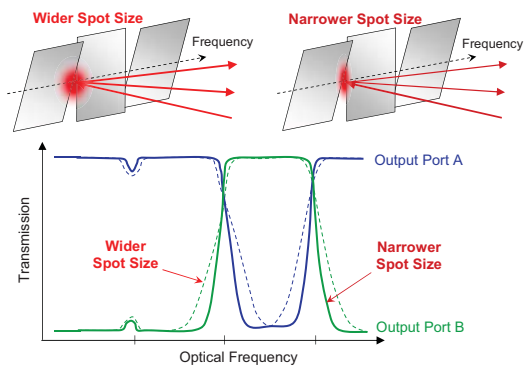

Figure 4-9: In a MEMS-based WSS, the shape of the transfer function is largely determined by the relative width of the light beam impinging on the mirror. Smaller spot sizes produce higher order Gaussian shaped channel transfer functions.

5 Other WSS Characteristics

5.1 Port Count

A single dimensional MEMS mirror array switch engine has the advantage that to increase the number of selectable ports, it is necessary only to increase the tilt angle or the mirror length of the MEMS mirrors. Provided this can be done, there is no limit to the number of ports that can be addressed. The height of the optics will increase as ports are added, but the footprint remains nearly the same, as shown in Figure 5-1.

An LCoS based switch engine has a limitation in that only a certain beam steering angle is practical. Thus, the way to increase port count is to increase the beam size on the LCoS engine (perpendicular to the wavelength dispersion direction). Beyond a certain point, this involves also increasing the beam width in the wavelength dispersion direction, which results in an increase in the optics footprint as shown in Figure 5-1.

The LC switching engine requires the addition of one more LC layer in the LC stack each time the number of ports is doubled. As the LC stack becomes thicker, the minimum beam size increases and the overall optics size increases. This leads to a stepwise increase in optics size as the number of ports increases beyond 2, 4, 8, or 16 ports.

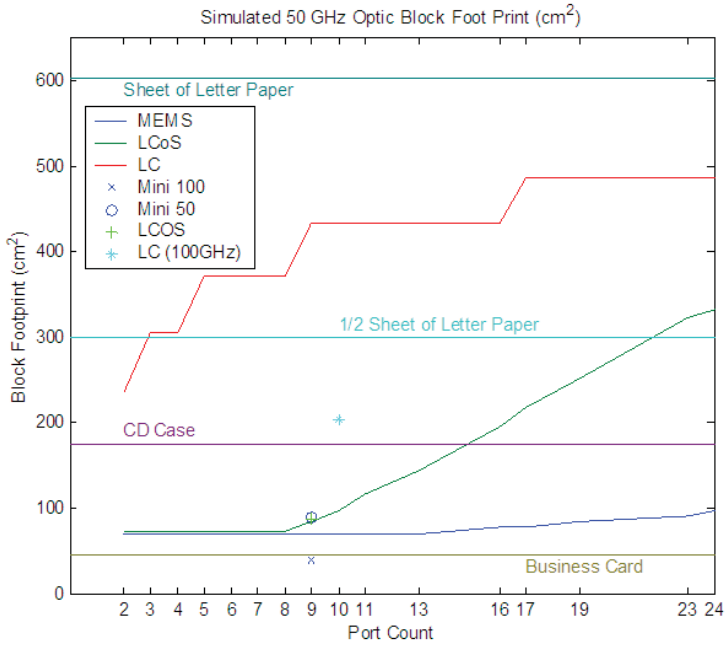

Figure 5-1: Optics footprint versus port count for various WSS switching engine technologies

5.2 Attenuation Accuracy

A single dimensional MEMS mirror array switch engine is subject to a certain amount of drift (slow angle change after a step voltage change) and aging (gradual angle changes independent of actuation history). These effects are not fundamental to the technology can be minimized through careful

design of the MEMS structures. Generally attenuation is achieved by offsetting the mirror from the optimal coupling position. In the attenuated state the attenuation can be very sensitive to the mirror angle, so even small changes in mirror angle are noticeable. Because of this, a single dimensional MEMS mirror array switch engine based WSS may have lesser attenuation accuracy specifications than other technologies. As MEMS technology improves, the attenuation accuracy is expected to continually and significantly improve. Also, through careful design at the system level, weaker attenuation accuracy can be accommodated and does not lead to system performance issues or significant limitations.

Attenuation accuracy of LCoS and LC switching engines are limited by the phase accuracy of the liquid crystal cells. The cells may change over time, particularly at elevated temperatures, resulting in changes in the attenuation versus voltage characteristics.

5.3 Switching Speed

A single dimensional MEMS mirror array switch engines can switch in a few tens of milliseconds; however the movement of one mirror can affect neighboring mirrors through pneumatic effects. For this reason the switching speeds are currently typically slowed to hundreds of milliseconds. However, these limitations are not fundamental and switching speeds of less than 10ms should be achievable if desired.

LCoS and LC based switching engines are limited by the response time of the liquid crystal fluid. The response time is a strong function of temperature, so the liquid crystal cells must be heated to avoid extremely slow response times at low temperatures. With a heater, response times can be tens of milliseconds. Multiple switching steps may be required to complete one switching operation however, particularly for LCoS where transitions must be carefully controlled to prevent crosstalk into unwanted ports during switching operations.

5.4 Advanced Features

An LCoS switch engine has the capability of enabling advanced features such as multicast switching (dividing the optical signal power into two or more ports at the same time) and variable passband widths (for example arbitrary selection of 50 GHz or 100 GHz channel spacings). The multicast switching comes at the expense of increased crosstalk into other ports. LC engines are capable of some signal splitting between ports, but only between a subset of port pairs, for example in an 8 port device signals can be split between only 12 of 28 possible port pair combinations.

5.5 Customization of Switching Engine

Single dimension MEMS mirror array and LC switch engines are designed specifically for WSS applications, allowing arbitrary selection of many properties such as number of pixels and pixel sizes and locations which can be selected to optimize the overall size and performance of the WSS. The LCoS and DLP based switching engine uses a pixel pattern developed for display applications (custom pixel arrangements are possible but the development is very expensive because of the need to redesign the underlying driving circuitry). Thus the availability of these engines is somewhat dependent upon the display market, and WSS designers may be limited in their design options such as the size and number of pixels in the switching engine.

LC and LCoS based switch engines are often advertised as being low cost by virtue of piggybacking on high volume production for commercial applications. However, commercial display applications use visible light while a WSS must operate at infrared wavelengths. To operate at infrared wavelengths, the liquid crystal fluid thickness must be increased, the antireflection coatings must be redesigned, and voltage driving techniques must be carefully chosen to prevent flickering (which is acceptable in

display applications because of the eye's limited response time). These differences mean that LC and LCoS based switch engines are significantly different from the commercial versions, and are essentially custom products subject to their own cost versus volume dependencies some what independent of the commercial products.

6 Summary

In summary, critical characteristics of a WSS, namely the component's size, its port isolation, and its channel bandwidth, are significantly determined by two fundamental properties of the switch engine technology utilized within the WSS: the minimum spot size achievable on the actuator and the amount of scatter occurring from the actuator. Because of the pixelated structure of the LCoS and DLP engines and the longitudinal thickness of the LC switch engine, the minimum spot size is fundamentally limited. However, the limitation on the spot size on the single dimension MEMS mirror array is limited by the surface quality of the mirror coating and considerably smaller spot sizes can be achieved. For similar reasons, the MEMS mirror also fundamentally generates less scatter than the other engine types. Therefore, WSS components build using single dimension MEMS mirror arrays can exhibit better port isolation performance, wider cascaded channel bandwidth, and smaller component sizes with larger port counts than can WSS components utilizing the other engine technologies.

7 References

1. M. Knapczyk et. al., "Reconfigurable Add–Drop Optical Filter Based on Arrays of Digital Micromirrors", *IEEE J. Lightwave Tech. 26* (2008), pp. 237-242.
2. D. Marom et. al., "Wavelength-Selective 1 K Switches Using Free-Space Optics and MEMS Micromirrors: Theory, Design, and Implementation", IEEE J. *Lightwave Tech. 23* (2005), pp. 1620-1630.
3. G. Baxter et al., "Highly programmable Wavelength Selective Switch based on Liquid Crystal on Silicon switching elements", *Proc. OFC/NFOEC* (2005)
4. Jack Kelly, "Application of Liquid Crystal Technology to Telecommunication Devices", *Proc. OFC/NFOEC* (2006), paper NThE1.
5. P. Wall, et al., "WSS Switching Engine Technologies" in *Proceedings OFC/NFOEC* (2008), paper OWC1.
6. R. Shankar, et al., "Multi-degree ROADM based on wavelength selective switches: Architectures and Scalability," *Opt Comm* 279 (2007), pp. 94-100.
7. B. Mikkelsen, et al., "Partial DPSK with excellent filter tolerance and OSNR sensitivity," *Electron Lett.* 42 (2006), pp. 1363-1365.
8. F. Heismann et. al, "43-Gb/s NRZ-PDPSK WDM Transmission with 50-GHz Channel Spacing in Systems with Cascaded Wavelength-Selective Switches" in *Proceeds of OFC/NFOEC* (2009), paper OThC1.
9. B. Collings, et. al., "Dependence of the Transmission Impairment on the WSS Port Isolation Spectral Profile in 50GHz ROADM Networks with 43Gb/s NRZ-ADPSK Signals" in *Proceedings of OFC/NFOEC* (2009), paper OThJ3.